9-1-2021

Turbulent Flow between Concentric Rotating Cylinders.

M. Mohamed
Mechanical Power Engineering Department., Faculty of Engineering., El-Mansoura University., Mansoura., Egypt., msafwat@mans.edu.eg

Follow this and additional works at: https://mej.researchcommons.org/home

TURBULENT FLOW BETWEEN CONCENTRIC ROTATING CYLINDERS

M. S. Mohamed
Mechanical Power Engineering Department,
Faculty of Engineering, Mansoura University.

الانسياب المضطرب بين اسطوانتين دوارتين متحدتى المركز .

الخلاصة:

يقدم هذا البحث دراسة نظرية للانسياب المضطرب بين اسطوانتين منحدتى المركز تدوران معا فى نفس الاتجاه أو فى اتجاهين متضادين بسرعات دوران مختلفة. تم عمل برنامج حاسب آلى لحل المعادلات التى تحكم حركة الانسياب. كما تم استخدام نموذج رياضى للاضطراب بعد عمل التعديلات اللازمة للأخذ فى الاعتبار وحدود جدران الاسطوانتين وكذلك دورانهما. تم دراسة تأثير تغير كل من النسبه بين القطرين ورقم رينولدز فى تجاه المحور على معامل الاحتكاك الهيدروليكى للهواء. تم التنبؤ بتوزيعات السرعة المتوسطة فى اتجاه المحور والاتجاه المماسى للاسطرانة وكذلك كثافة الاضطراب واجهاد القص. وقد أوضحت المقارنة بين النتائج الحالية ونتائج أخرى مماثلة اتفاقا واضحا.

ABSTRACT:

The turbulent flow between concentric cylinders both rotating in the same or opposite directions is investigated theoretically. A finite difference scheme is developed to solve the boundary layer equations covering the flow. A two-equation model of turbulence was employed in this study. Modifications have been made to the model to take into account the effect of rotation of the cylinders and the existing of the wall. The effect of changing the radius ratio, axial Reynolds number and angular velocity ratio on the hydraulic friction head loss of air is studied. Distributions for axial mean velocity, tangential mean velocity, turbulence intensity and shear stress in both the entrance region and fully developed region are predicted, also. Comparisons of the present numerical results with other investigators results show good agreement.

1.INTRODUCTION:

Turbulent flow between concentric cylinders (one of them rotating) occurs in various rotating machinery such as journal bearing, axial flow between the stationary and rotating parts of turbo-machines and the flow in the rising line of deep well pumps. One of the important examples is the cooling system of gas turbine rotor, where some portion of the cooling air can be supplied to the rotor area through an annular duct, formed by two coaxial cylinders, with the inner cylinder rotating. Flow in such system can be characterized by very high Reynolds number ($R_e \approx 10^6$). Most of papers dealing with this type of flow analyze the problem in the range of low or moderate R_e, in an effort to explain the nature of Taylor vortices and to quantify their complex effects. There are very few data, both experimental and theoretical, from the rang of high R_e.

The papers of Yamada [1,2] are dealing with high rotational R_e and axial throughflow. Kaye and Elgar [3] used the axial Reynolds number (R_e) and Taylor number as criteria, characterizing the flow, to distinguish four distinct flow regimes. These regimes are laminar

flow, laminar flow with Taylor vortices, turbulent flow and turbulent flow with Taylor vortices. The boundaries of the regimes were conveniently represented by a plot of the axial Reynolds number versus Taylor number. The experiments of Kaye and Elgar [3] were extended to higher Reynolds and Taylor numbers by Kosterin, Koshmanow and Finatyew, and are quoted in [4].

Mansour [5] investigated theoretically the hydraulic resistance in an annulus of concentric rotating cylinders. The axial and tangential velocity distributions were introduced. He assumed that the annulus is long enough and a uniform purely developed laminar flow is considered. He found that rotation affects the friction coefficient as well as the axial and tangential velocity distributions. He concluded that the friction coefficient for an annulus of rotating walls is higher than that for stationary walls. Also, the friction coefficient ratio increases with the increase of both speed ratio ($\omega r/u$) and the relative angular velocity ratio (ω_1/ω_2).

Boubnov et al [6] investigated the stability conditions of the flow between two concentric cylinders with the inner one rotating. They employed a fluid with axial, stable linear density stratification. They used a gap of radius ratio 0.275. Experiments show that stratification has stabilizing effect on the flow with the critical Reynolds number depending on the buoyancy frequency of the fluid. The selected vertical wave length at onset of instability is reduced by stratification effect and is for the geometry considered only about half the gap width. They devided the flow regimes into three regimes depending on both Reynolds number and Froud number.

Although the stability of supercritical circular couette flow has been studied extensively, results for the velocity field of the flow are limited. Recently, the azimuthal velocity profiles for the Taylor vortex, wavy vortex and turbulent Taylor vortex flow in the annulus between a rotating inner cylinder and a fixed outer cylinder with fixed end conditions were measured using laser Doppler velocimetry by Wereley and Lueptow [7]. They measured the azimuthal velocity at several points distributed at both radial and axial directions for several Reynolds number. Increasing Reynolds number indicated that: the magnitude of the radial gradient of azimuthal velocity near both cylinders increases and the radial outflow region between pairs of vortices becomes increasingly jet-like.

The present investigation is concerned with the theoretical study of the development of turbulent flow in concentric annulus at different conditions such as rotating the inner and outer cylinders in the same or opposite directions at different velocity ratios. Steady axial flow is assumed to exist under a constant axial pressure gradient. The aim of this study is to develop a finite difference scheme using the available turbulence models to predict the flow patterns and its effect on the hydraulic loss coefficient.

2. GOVERNING EQUATIONS:

Assuming that the fluid has constant physical properties and the flow is steady axisymmetric with the absence of body forces. The equations governing the fluid motion of an annulus with rotating cylinders and axial throughflow, in cylindrical polar coordinates, are:

r-momentum equation:

$$V_r \frac{\partial V_r}{\partial r} - \frac{V_n^2}{r} + V_z \frac{\partial V_r}{\partial z} = -\frac{1}{\rho}\frac{\partial P}{\partial r} + \nu\left[\frac{1}{r}\frac{\partial}{\partial r}\left(r\frac{\partial V_r}{\partial r}\right) - \frac{V_r}{r^2} + \frac{\partial^2 V_r}{\partial z^2}\right] \quad \text{......... (1)}$$

θ -momentum equation:

$$V_r \frac{\partial V_\theta}{\partial r} + \frac{V_r V_\theta}{r} + V_z \frac{\partial V_\theta}{\partial z} = v \left[\frac{1}{r} \frac{\partial}{\partial r} \left(r \frac{\partial V_\theta}{\partial r} \right) - \frac{V_\theta}{r^2} + \frac{\partial^2 V_\theta}{\partial z^2} \right] \dots\dots (2)$$

z -momentum equation:

$$V_r \frac{\partial V_z}{\partial r} + V_z \frac{\partial V_z}{\partial z} = -\frac{1}{\rho} \frac{\partial P}{\partial z} + v \left[\frac{1}{r} \frac{\partial}{\partial r} \left(r \frac{\partial V_z}{\partial r} \right) + \frac{\partial^2 V_z}{\partial z^2} \right] \dots\dots (3)$$

Continuity equation:

$$\frac{\partial (r V_z)}{\partial z} + \frac{\partial (r V_r)}{\partial r} = 0 \dots\dots (4)$$

Scalar property ϕ:

The transport equation of the scalar quantities: turbulent kinetic energy k, its dissipation rate ε and the Reynolds stresses in a general from is:

$$\rho \frac{\partial}{\partial z} (r V_{z\phi}) + \rho \frac{\partial}{\partial r} (r V_{r\phi}) = -\frac{\partial}{\partial r} (r J_\phi) + P_\phi - D_\phi \dots\dots (5)$$

where ϕ is the required scalar quantity. J_ϕ is the flux of the scalar property ϕ, P_ϕ is the generation rate of ϕ and D_ϕ is the dissipation rate of ϕ. The velocity components (V_z, V_r and V_θ) and the scalar property ϕ represent time average values.

Applying the well known Prandtl boundary layer assumptions and check the order of magnitude of each term of the above equations [8], equations (1), (2) and (3), which represent the momentum equations for the flow in the entry region, may be reduced to the following simplified boundary layer equations:

$$\rho \frac{V_\theta^2}{r} = \frac{\partial P}{\partial r} \dots\dots (6)$$

$$V_r \frac{\partial V_\theta}{\partial r} + V_z \frac{\partial V_\theta}{\partial z} = \frac{v}{r} \frac{\partial}{\partial r} \left(r \frac{\partial V_\theta}{\partial r} \right) \dots\dots (7)$$

$$V_r \frac{\partial V_z}{\partial r} + V_z \frac{\partial V_z}{\partial z} = -\frac{1}{\rho} \frac{\partial P}{\partial z} + v \left[\frac{1}{r} \frac{\partial}{\partial r} \left(r \frac{\partial V_z}{\partial r} \right) + \frac{\partial^2 V_z}{\partial z^2} \right] \dots\dots (8)$$

The fully developed flow, which occurs if the annulus is sufficiently long, provides an analytical check on the finite difference solution to be obtained. After passing the initial section, all derivatives in the axial direction become zero, except the constant pressure gradient $(\partial/\partial z) = 0$. Additionally, there are no variation in the tangential direction $(\partial/\partial\theta) = 0$, because of the axial symmetry of the system. With these simplifications and the assumptions of negligible dissipation rate and no body forces, except the centrifugal force, the equations of conservation for an incompressible turbulent flow will take the form:

$$A_J^D = \left(D + (C/2) \right)_{J.}^D \qquad\qquad A_J^D = A_J^U + A_{J.}^D + A_{J.}^D.$$

$$B_J = \int_{X^0}^{X^U} \int_{\eta_-}^{\eta_.} r\delta\, S_\phi\, dz\, d\eta = \bar{s}_\phi\, Volum. \qquad (Volume = r\delta\, \nabla z\, \nabla\eta)$$

where $\bar{s}_\phi$ = Average source (sink) value over the control volume.
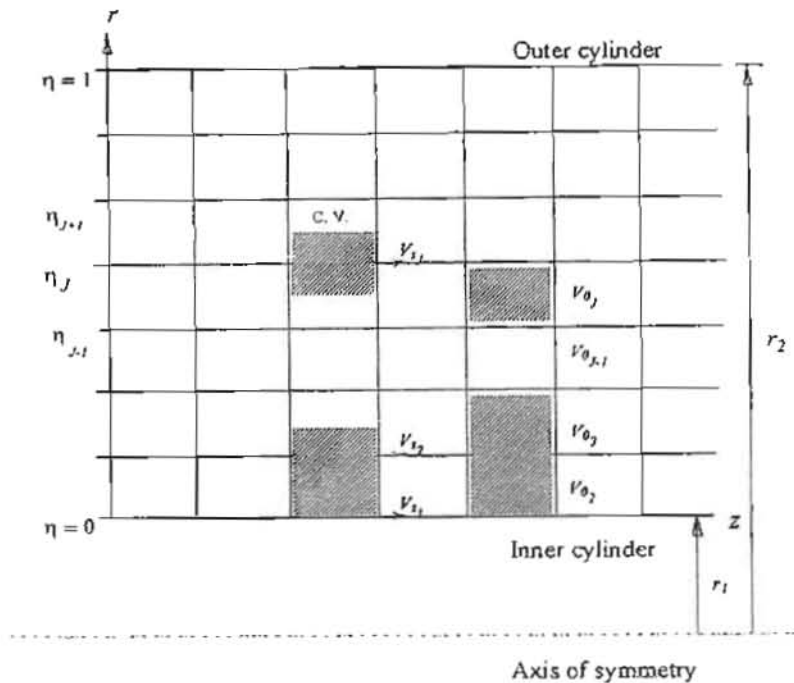

Figure (i) Mesh network and control volumes for finite difference representation

Integrating the continuity equation over the V_z-control volume gives:

$$\left[(\rho r\delta V_r \nabla\eta)_J^D - (\rho r\delta V_r \nabla\eta)_J^U \right] + \left[\rho r(V_\theta - GV_r)\nabla z \right]_. - \left[\rho r(V_\theta - GV_r)\nabla z \right]_. = 0 \quad\text{...... (19)}$$

$(V_\theta)_+$ equals to $(V_\theta)_{J+1}$ and $V_.$ equals to $(V_\theta)_{J-1}$.

The equation of V_z can be obtained by replacing ϕ by V_z in equation (18), as follows:

$$A_J^D\,(V_z)_J^D = A_J^U\,(V_z)_J^U + A_{J.}^D\,(V_z)_{J+1}^D + A_{J.}^D\,(V_z)_{J-1}^D + B_J \quad\text{.................... (20)}$$

where the constants A are coefficients of integration, superscript U denotes upstream conditions while D denotes downstream conditions and B_J is:

$$B_J = -(r\delta)_J^D\, \nabla z\, \nabla\eta\, \left(\overline{dP/dz}\right)$$

In confined flow $(\overline{dP/dz})$ is not known. An estimated pressure field $(\overline{dP/dz})^*$ is used with the transport equation of V_z-momentum to obtain a preliminary V_z-velocity distribution, say $((V_z)_J^D)^*$. This velocity field satisfies the momentum equation but it does not satisfy the

continuity equation. The pressure and velocity are then corrected in the following way [13]: To estimate the mass-flux imbalance at each node, a velocity correction $((V_z)_j^D\,)'$ was added to $((V_z)_j^D\,)^*$ in order to satisfy the continuity equation. An approximate relation between $((V_z)_j^D\,)'$ and the corresponding pressure correction $(\overline{dP/dz}\,)'$ can be obtained from u-momentum equation. Solving both equations will lead to the pressure and velocity corrections, $((V_z)_j^D\,)'$ and $(\overline{dP/dz}\,)'$ respectively. Better approximations for the pressure gradient and the velocity field can be obtained as:

$$\overline{dP/dz} = (\overline{dP/dz}\,)^* + (\overline{dP/dz}\,)' \quad \dotfill (21)$$

$$(V_z)_j^D = ((V_z)_j^D\,)^* + ((V_z)_j^D\,)' \quad \dotfill (22)$$

The new velocity field satisfied the continuity equation exactly. But, the substitution with the new pressure gradient in the V_z-momentum equation will lead to a velocity field which does not satisfy continuity equation exactly. An iterative procedure is needed before marching downstream to the next cross-stream plane until the difference is less than 0.3%.

By the same manner, equation of V_θ is:

$$A_{j,v}^D\,(V_\theta)_j^D = A_{j,v}^U\,(V_\theta)_j^U + A_{j,v}^D\,(V_\theta)_{j+1}^D + A_{j,v}^D\,(V_\theta)_{j-1}^D + B_{j,v} \quad \dots\dots (23)$$

where $\quad\quad B_{j,v} = -(r\,\delta)_j^D\,\nabla_z\,\nabla\eta\,\left(P_{j-1}^D - P_j^D\right)$

A-coefficients and B-coefficient have the subscript V_θ because they are obtained from integration of equation (5) over the V_θ-control volume. The pressure fluctuation P_j^D is unknown. The same procedure in finding the pressure gradient and V_z-field is followed also to find the pressure fluctuation and the V_θ-field from V_θ-momentum equation. It gives:

$$P_j^D = (P_j^D\,)^* + (P_j^D\,)' \quad \dotfill (24)$$

$$(V_\theta)_j^D = ((V_\theta)_j^D\,)^* + ((V_\theta)_j^D\,)' \quad \dotfill (25)$$

4.1. Initial and Boundary Conditions:

Uniform axial velocity profile is assumed at the inlet of the annulus and equals to the mean velocity. The radial and tangential velocity profiles are assumed to be zero. The initial distribution of turbulent kinetic energy k and its dissipation rate ε are assumed be to uniform and equal to that values given by Launder and Spalding [14] for turbulent pipe flows. All velocity components along the inner and outer radiuses are assumed to be zero, expect for the tangential mean velocity at the wall of the inner and outer cylinders. For an annulus having an inner cylinder of radius r_1 and rotates with angular velocity ω_1 while its outer cylinder is of radius r_2 and rotates, also, with angular velocity ω_2, the flow is subjected to the following boundary conditions:

at inlet section $(z=0)$ and $r_1 < r < r_2$ $\quad V_z = \overline{V_i}$ (flat profile at entrance)
$\quad\quad\quad k = 0.003\,V_i^2$, $\varepsilon = C_\mu\,k^{2/3}\,/\,(0.03\,r_h)$ and $P = P_0 = -V_i^2\,/\,2$
at the walls $z \geq 0$ and $r = r_1$ $\quad\quad V_r = V_z = 0$ and $V_\theta = \omega_1\,r_1$
$\quad\quad\quad\quad\quad z \geq 0$ and $r = r_2$ $\quad\quad V_r = V_z = 0$ and $V_\theta = \omega_1\,r_2$
fully developed flow $\partial/\partial z = 0.0$ except $(\partial P/\partial z \neq 0.0)$

4.2.Near Wall Treatment :

The k-ε is valid only in high Reynolds number flows far from the viscous flow near the wall. Therefore, special treatment is needed to take into account the effect of fluid viscosity on turbulence, particularly, wall shear stress τ_w, the production of turbulence energy k and its dissipation ε near the wall. The procedure is based on the analytical solutions of the thin Coutte-flow type region which extends from $r^+ \approx 30$ to the wall, where $(r^+ = r\, \tau_w/v)$. This procedure is biased on the assumption that the Log-law:

$$\frac{V_\theta}{(V_\theta)_\tau} = \frac{1}{\kappa}\, ln\,(E\, r^+) \qquad \text{.................................. (26)}$$

is valid over the uniform shear stress region ($0 < r^+ < r_p^-$) where

$(V_\theta)_\tau = \sqrt{\tau_w/\rho}$, $\kappa = 0.42$ (Von Karman constant) and $E = 9.0$ for smooth walls.
Using the simplification [11]

$$\tau_p\, (= \tau_w) = \rho\; C_\mu^{1/2}\, k_P$$

to calculate $(V_\theta)_P$ the wall shear stress τ_w can be obtained as:

$$\tau_w = \rho\, \kappa\; C_\mu^{1/4}\; k_P^{1/2}\; \left[(V_\theta)_w - (V_\theta)_P\right] \,/\, ln\,(E\, r_P^+) \qquad \text{.................... (27)}$$

$$r_P^+ = \rho\, r_P\; C_\mu^{1/4}\; k_P^{1/2}/\mu \qquad \text{.................................. (28)}$$

subscripts p and w denotes the node p and the wall conditions, respectively. In equation (27), the quantity $[(V_\theta)_w - V_\theta)_P]$ is employed to account for the rotation of walls.

The production of turbulence near the wall can be obtained from transport equation k. It was modified in order to take into account the effect of wall shear stress τ_w. From equation (16) the term, $-\overline{v_z\, v_r}\, (\partial V_z/\partial r)$, is the dominated part of P_k and is denoted as P_k'.

$$P_k' = -\overline{v_z\, v_r}\, \frac{\partial V_z}{\partial r} = \frac{\tau_w}{\rho}\, \frac{\partial V_z}{\partial r} = \frac{\tau_w}{\rho}\, \frac{(V_\theta)_\tau}{\kappa r}$$

therefore,
$$P_k' = \tau_w^{3/2}\, /\rho^{3/2}\, \kappa\, r \qquad \text{.................................. (29)}$$

The dissipation rate near the wall, ε', was obtained from the assumption that the length scale of turbulence is $L = k^{3/2}/\varepsilon$ which is related to the mixing length as $L = C_\mu^{3/4}\, \kappa\, r$, thus,

$$\varepsilon' = C_\mu^{3/4}\; k_P^{3/2}\, /\kappa\, r \qquad \text{.................................. (30)}$$

5. RESULTS AND DISCUSSION:

The axial air flow in four gaps, at radius ratio of 0.333, 0.5, 0.6 and 0.75, rotating at wide range of angular velocity ratios is used in this study. Positive and negative angular velocity ratios as well as inner cylinder rotating only and outer cylinder rotating only were investigated to give a range of flow Reynolds number $6.62 \times 10^5 \le R_e \le 16 \times 10^6$ and rotational Reynolds numbers $2.43 \times 10^3 \le R_\theta \le 48 \times 10^4$. The effect of these parameters on the flow

pattern and friction head loss was studied. In all numerical computations a non-uniform grid in the radial direction is employed depending on the axial velocity gradient. Twenty nodes in the radial direction were used to give grid-independent solution for this flow. Five iteration were found to give a converging solution.

5.1. *Loss Coefficient in Rotating Concentric Pipes:*

In all the test runs axial Reynolds number R_e was higher than 10^5, so the flow is turbulent when both pipes are held stationary. Therefore, for $R_\theta = 0$, the friction head loss coefficient is equal that value calculated from Blasius equation for smooth pipes $f = 0.3164\ R_r^{0.25}$.

When rotation begins, it is obvious that $\lambda = (\tau_{rz})_w / (1/2)\ V_z^2$ deviates gradually from f. Rotational hydraulic friction head loss λ increases with increasing the aspect ratio (l/b) and reaches a constant value at $l/b = 50$.

Figure (1) shows the variation of the friction coefficient ratio λ/f with radius ratio at different angular speed ratios α for aspect ratio ($l/b = 50.0$). The figure indicated that increasing the angular velocity ratio increases the friction coefficient ratio (R_θ /R_e increases). For constant angular velocity ratio and constant axial velocity $V_z = 50$ (m/s), it is clear that λ/f increases with increasing the radius ratio figure (1-a). For the case when outer cylinder is rotating only ($\omega_1 = 0$), increasing the radius ratio has an opposite effect on λ/f where it decreases with increasing the radius ratio as shown in figure (1-b). This can be explained as, increasing the radius ratio decreases the tangential velocity gradient which in turn reduces the friction coefficient ratio. The figure shows that the friction coefficient ratio is greater than unity ($\lambda/f \geq 1$).

The change of the friction coefficient ratio λ/f with axial Reynolds number R_e in a gap at radius ratio $= 0.5$ for different angular velocity ratios is presented in figure (2). Figure (2-a) shows that for constant angular velocity ratio, λ/f increases with increasing R_e (R_θ /R_e decreases as R_θ is constant). For outer cylinder rotating only ($\omega_1 = 0$) shown in figure (2-b), λ/f increases with increasing the angular velocity ω_2 also, while it decreases with increasing the R_e (or decreasing R_θ /R_e).

The variation of the friction coefficient ratio with the rotational speed ratio ~... be explained by examining the velocity profiles in the gap of the rotating cylinders.

5.2. *Mean Velocity Distribution and Turbulence Intensity:*

The development of the flow parameters with the downstream distance for a gap having radius ratio 0.75; rotating at angular speed ratios $\alpha = -2$, outer cylinder rotating only, inner cylinder rotating only and $\alpha = 4$; are presented in figures (3 to 6) respectively. Comparison between the flow parameters for stationary (dashed lines) and rotating cylinders (solid lines) are presented. The dimensionless mean axial and tangential velocity profiles [$V_z /(V_z)_{max}$ and $V_\theta /(V_\theta)_{max}$], turbulence intensity profiles $\sqrt{\overline{v_r'^2}} /(V_z)_{max}$ and shear stress distribution $\overline{v_r v_r} / (V_z)^2_{max}$ in the gap verses the dimensionless radial distance $(r - r_1)/(r_2 - r_1)$ are predicted for aspect ratio $l/b = 50$. Seven downstream stations ($z/L = 0.04, 0.12, 0.3, 0.45, 0.6, 0.75$ and 1.0 respectively) for a flow at axial Reynolds number $R_e = 6.62 \times 10^5$ were chosen. The dimensionless axial mean velocity $V_z /(V_z)_{max}$ was found to be self-

similar after z/L = 50. The velocity profiles $V_z/(V_z)_{max}$ change along the annulus, as shown in the figures, for various values of R_θ. The axial mean velocity profiles remain flat up to distance z/L = 0.30. As z/L increases, the velocity profiles deform gradually, due to a stabilizing effect of the centrifugal force of the swirling flow. Lavan et al [15] indicated in their theoretical work that reverse flow is to be expected near the wall at the entrance region of the pipe, for large R_θ. At z/L = 50 and more downstream, the velocity profiles become approximately independent of the axial distance from the inlet. For a gap at constant radius ratio, the comparison between the mean axial velocity profiles at deferent angular velocity ratios indicated that the maximum velocity tends to move far from the axis of rotation as the angular velocity ratio increases while it is not affected by increasing axial Reynolds number R_e, as shown in figure (8-a). For constant angular velocity ratio, increasing the radius ratio tends to shift the maximum axial velocity towards the axis of rotation as shown in figure (9-a), which agrees with Mansour [5] for laminar flow.

Figure (7) shows the response surface for the development of the dimensionless tangential mean velocity $V_\theta/(V_\theta)_{max}$ for different angular velocity ratios for a gap at radius ratio 0.6 and axial Reynolds number $R_e = 6.62 \times 10^5$.

When both cylinders are rotating at opposite directions at $\omega_1/\omega_2 = -2$ and axial Reynolds number $R_e = 6.62 \times 10^5$, the flow at every point is turbulent. Figure (3-b) shows that, the tangential mean velocity distribution near both cylinder walls is sharply inclined, whereas it is much less than that in the middle of the gap. As R_θ is increased, this trend is more noticed. The turbulence intensity $\sqrt{v_t'^2}/(V_z)_{max}$ figure (3-c), shows a peak near both cylinder walls. It was found that, this peak value increases as R_θ grows larger. Yamada [16] noticed that, once R_θ exceeds 5040, the fluid is divided into two distinct regions of laminar and turbulent flows. This is the formation of a so-called spiral turbulence in which a laminar flow portion and turbulent flow portion coexist like a double-screw pattern. He also noticed that, when both cylinders rotate in opposite directions, Taylor vortices and spiral turbulence develop simultaneously or one after the other, depending upon the rotational Reynolds number R_θ, and they coexist in the gap.

When the outer cylinder is rotating at $R_\theta = 7274$ while the inner one is stationary ($\omega_1 = 0$), the turbulence intensity $\sqrt{v_t'^2}/(V_z)_{max}$, sharply increases as shown in figure (4-c) and the velocity gradient (v) increases slightly, figure (4-b). Yamada [16], found the same phenomenon in his experiment, and he noticed that the flow becomes spiral turbulence.

Figure (5) shows an axial flow at $R_e = 6.62 \times 10$ with the inner cylinder rotating at $R_\theta = 2425$ while the outer cylinder is stationary ($\omega_2 = 0$). The tangential mean velocity profile, figure (5-b), shows a flat portion, in the meddle, up to z/L = 0.6. The velocity distribution shows self-similarity case after l/b= 50. The turbulence intensity $\sqrt{v_t'^2}/(V_z)_{max}$ figure (5-c), has a peak value near the inner cylinder and the axis of the flow tends to move towards the outer cylinder. This peak value decreases with increasing both the radius ratio and the axial Reynolds number R_e. These results agree well with that obtained with El-shaarawi et al [17] for turbulent flow in an annulus with inner cylinder rotation.

When the outer cylinder and the inner cylinder are rotating in the same direction ($\alpha=\omega_1/\omega_2 = 4$), shown in figure (6-b), the tangential mean velocity profile indicated two peak values near the rotating walls with high velocity gradient. The velocity gradient reduces as the flow goes downstream. The turbulence intensity, figure (6-c), increases gradually from the outer to the inner cylinder and it has a steep change near the inner one. In the fully

developed region, the flow is stabilized and Yamada [16] found that, the flow is laminar even at R_θ =5000, because the laminar flow regime increases up to a high R_θ as the angular velocity ratio approaches unity.

5.3. Shearing Stress:

The dimensionless shear stress, $\overline{v_t\,v_z}/(V_z)^2_{max}$, increases as the flow goes down-stream as shown in figure (3-d). It decreases with increasing both the radius ratio and axial Reynolds number, figures (8 and 9). The shear stress was found to be reduced as the rotational Reynolds number increases. In the case of outer cylinder rotating while the inner cylinder is fixed, an opposite trend is obtained.

6. CONCLUSIONS:

Nonswirling turbulent axial flow between two concentric rotating cylinders was studied numerically. The flow pattern and the hydraulic resistance in the gap were investigated in the ranges of flow axial Reynolds number $6.62 \times 10^5 \le R_e \le 5.16 \times 10^6$ and rotational Reynolds numbers $2.43 \times 10^3 \le R_\theta \le 7.48 \times 10^4$. The flow parameters in both entrance and fully developed regions were predicted.

The results can be concluded in the following points:

1) For constant axial Reynolds number R_e, the hydraulic friction coefficient, λ/f, in the initial region is function the rotational Reynolds number R_θ and the downstream distance z/L while after z/L > 50, it depends on the rotational Reynolds number R_θ, only.
2) In the fully developed region, the hydraulic friction coefficient increases with increasing (R_θ /R_e). For the same the angular velocity ratio, it increases with increasing both (R_θ /R_e) and radius ratio r_1/r_2. It is generally less than unity except for the case of the cylinders rotating in opposite directions.
3) In the case of outer cylinder rotating while the inner one is stationary; the friction coefficient ratio, λ/f, increases with increasing the angular velocity of the outer cylinder ω_2. For constant ω_2, the swirling velocity given to the flow by rotating the cylinder tends to shift the flow gradually to laminar flow which in turn reduces the friction head loss coefficient ratio. Reducing the radius ratio increase the rotating area which in turn allows the flow more to reach laminar flow case that decreases λ/f. The friction coefficient ratio, λ/f, is generally greater than unity.
4) The axial maximum mean velocity tends to shift towards the axis of rotation as the radius ratio increase while there is no effect of increasing the axial Reynolds number R_e on the location of the axial maximum velocity.
5) The turbulence intensity and shear stress reduce with increasing both the axial Reynolds number and radius ratio. The effect of increasing the rotational Reynolds number is to reduce both turbulence intensity and shear stress while they increase with increasing ω_2 in the case of stationary inner cylinder.

7. NOMENCLATURE:

b	Gap width = $r_2 - r_1$.
$C_{\varepsilon 1}, C_{\varepsilon 2}$	Constants in the k-ε model.
$C_{\varepsilon 3}$	Constant for the additional dissipation term.
C_μ	Eddy viscosity coefficient.
f	Hydraulic friction coefficient for stationary cylinder.

k	Turbulent kinetic energy.
L	Pipe length.
P_k	Production term in the k transport equation.
R_e	Axial Reynolds number $= 2Ub/v$.
R_θ	Rotational Reynolds number $= |\omega_2 - \omega_1|(r_2^2 - r_1^2)/2v$.
r	Arbitrary radius in the gap.
r_h	Hydraulic radius $= 2(r_2 - r_1) = 2b$.
r_1, r_2	Radius of inner and outer cylinder respectively.
$M = r_1/r_2$	Radius ratio.
r, θ, z	Cylindrical coordinate system.
T_k, T_ε	Diffusion term in k transport equation and ε transport equation respectively.
V_z, V_θ, V_r	Axial, tangential and radial mean velocity respectively.
v_z, v_θ, v_r	Axial, tangential and radial turbulence fluctuation component respectively.
v, v_r	Reynolds shear stress.
ε	Dissipation rate of the turbulent kinetic energy k.
ω	Angular velocity.
ρ	Fluid density.
μ	Fluid dynamic viscosity.
v	Fluid kinematic viscosity.
v_t	Turbulent eddy viscosity.
$\sigma_{k,t}, \sigma_{\varepsilon,t}$	Turbulent Prandtl number in k and ε transport equations.
τ	Shear stress.
α	Angular velocity ratio $= \omega_1/\omega_2$.
λ	Rotational hydraulic friction coefficient.

8. REFERENCES:

1-Yamada, Y., "Resistance of a Flow Through an Annulus with an Inner Rotating Cylinder," *Bulletin of J.S.M.E.*, Vol. 5, No. 18, 1962, PP. 302-310.

2-Yamada, Y., "Torque Resistance of a Flow Between Rotating Coaxial Cylinders Having Axial Flow," *Bulletin of J.S.M.E.*, Vol. 5, No. 20, 1962, PP. 634-642.

3-Kaye, J., and Elgar, E. C., "Modes of Adiabatic and Diabetic Fluid Flow in an Inner Rotating Cylinder," *ASME Transactions*, Vol. 80, 1958, PP 753-765.

4-Beranek, K., and Streda, J., "On the Flow of Viscous Liquids Through Annular Clearance with the Rotating Inner Cylinder," *Acta Technica CSAV*, No. 6, 1979, PP 665-676.

5-Mansour, H., "Laminar Flow Between Coaxial Rotating Cylinders," *Mansoura Engineering Journal (MEJ)*, Vol. 14, No. 2, Dec. 1989, PP M21- M41.

6-Boubnov, B. M., Gledzer, E. B., and Hopfinger, E. J., "Stratified Circular Couette Flow: Instability and Flow Regimes," *Journal of Fluid Mechanics*, Vol. 292, Jun. 1995, PP 333-358.

7-Wereley, S. T., and Lueptow, R. M., "Azimuthal Velocity in Supercritical Circular Couette Flow," *Experiments of Fluids*, Vol. 18, No. 1-2, Dec 1994, PP 1-9.

8-Astill, K. N., "Modes of Adiabatic Flow in the Entrance Region of an Annulus with an Inner Rotating Cylinder," *Ph.D. dissertation,* Massachusetts Institute of Technology, 1961.

9- Prandtl, L., "Bemerkungen zur Theorie der Frien Turbulenz", *Lenz. ZAMM,* Vol. 22, 1942, PP 241-243.

10- Kolmogorov, A. N., "Equations of Turbulent Motion of an Incompressible Fluid", *Itv. Ak. nauk SSR, Serıa Fizicheska,* VI 1942, No. 112, 1942, PP 56-58.

11-Patanker, S. V. and Spalding, D. B., "A Calculation Procedure for Heat, Mass and Momentum Transfer in Three-Dimensional Parabolic Flows," *International Journal of Heat and Mass Transfer,* Vol. 15, 1972, PP 1787-1806.

12-Jones, W. P., and Launder, B. E., "The Prediction of Laminarisation with a Two-Equation Model of Turbulence," *International Journal of Heat and Mass Transfer,* Vol. 15, 1972, PP 301.

13-Carretto, L. S., Gosman, A. D., Patanker, S. V. and Spalding, D. B., "Two Calculation Procedures for Steady, Three-Dimensional Flows with Recirculation," *Proceeding 3rd International Conference on Numerical Methods in Fluid Dynamics,* Springer-Verlag, New York, 1972, PP 60-68.

14-Launder, B. E., and Spalding, D .B., "The Numerical Computation of Turbulent Flows," *Computer Methods in Applied Mechanics and Engineering,* Vol. 3, 1974, PP 269-289.

15-Lavan, Z., Nielsen, H., and Fejer, A. A., "Separation and Flow Reversal in Swirling Flows in Circular Ducts," *Physics of Fluids,* Vol. 12, No. 9, 1969, PP 1747-1757.

16-Yamada, Y., and Imao, S., "Flow of a Fluid Contained Between Conceatric Cylinders Both Rotating," *Bulletin of J.S.M.E.,* Vol. 29, No. 252, 1986, PP. 1691-1697.

17-El-Shaarawi, M., and Sarhan, S., "Developing Laminar Free Convection in an Open Ended Vertical Annulus with a Rotating Inner Cylinder," *ASME Journal ˑ Fluid Engineering,* Vol. 103, Aug. 1981, PP 552-558.

18-Morcos. S. M., Abou-Ellail, M. M., Abou-Arab, T..W., "Combined Forced and Free Turbulent Heat Transfer in a Verical Annulus with Rotating Inner Cylinder," *3 rd International Conference on Methods in Thermal Problems,* Seattle, Washington, August, 1983, PP 762-777.
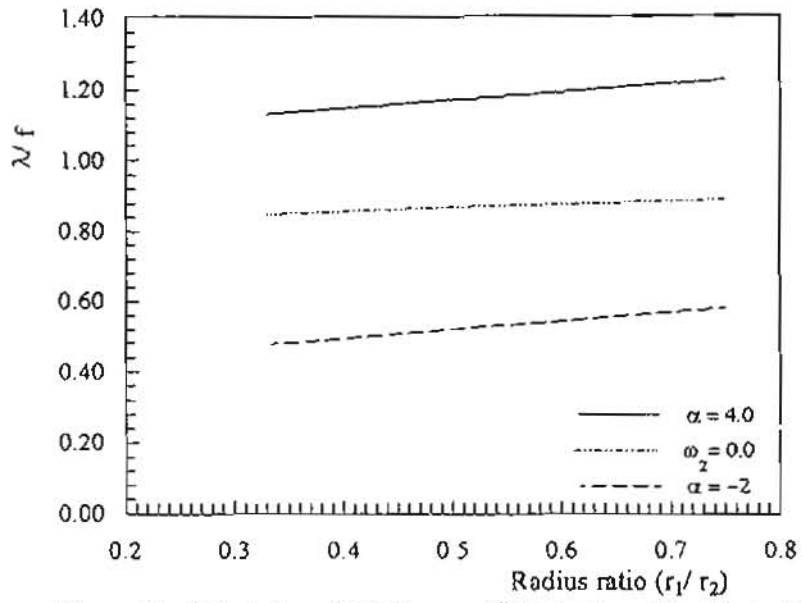
Figure (1-a) Variation of Friction coefficient ratio with radius ratio
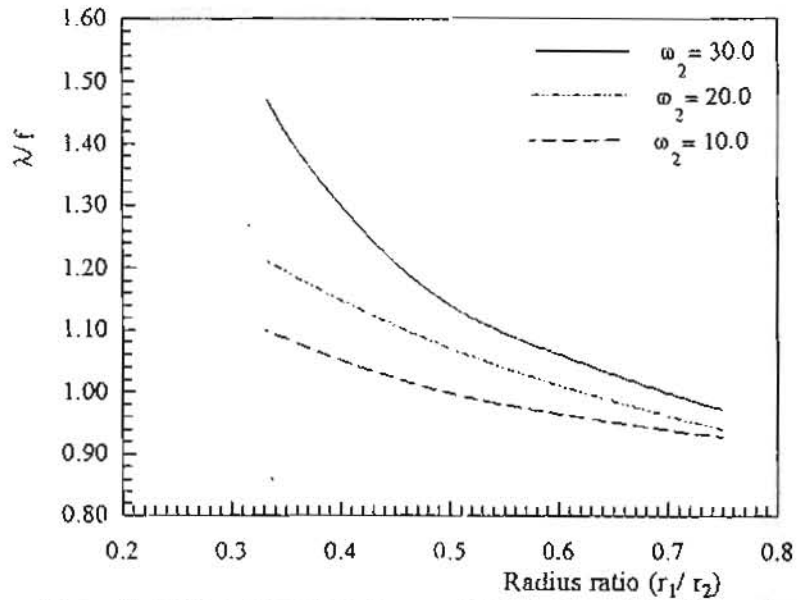at different angular velocity ratios for $V_{z_{mean}}$ = 50 (m/s)

Figure (1-b) Variation of friction coefficient ratio with radius ratio
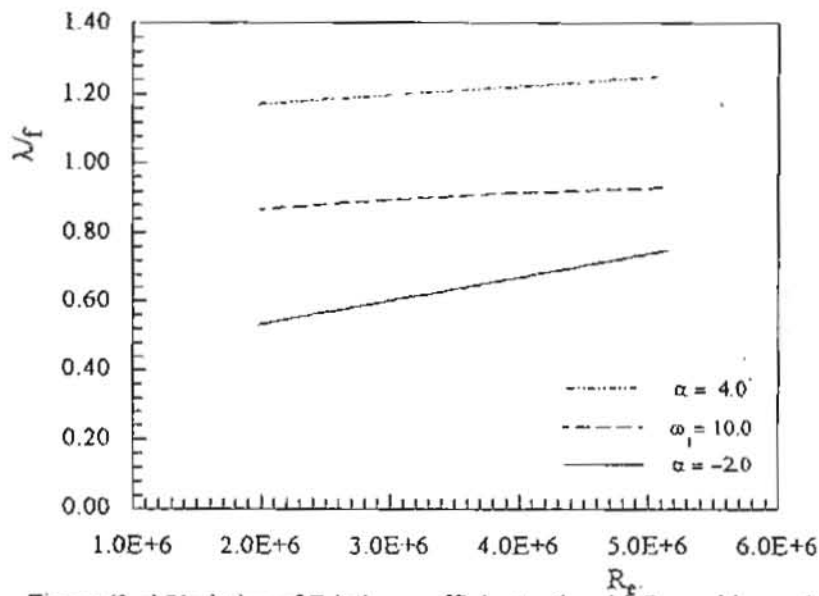for outer cylinder rotating only (ω_i = 0.0).

Figure (2-a) Variation of Friction coefficient ratio with Reynolds number
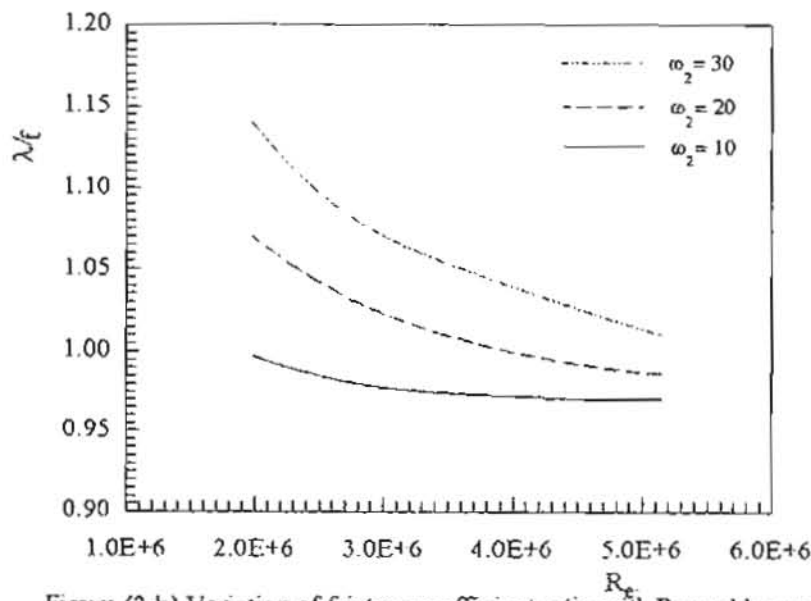for different angular velocity ratios for a gap of radius ratio = 0.5

Figure (2-b) Variation of friction coefficient ratio with Reynolds number
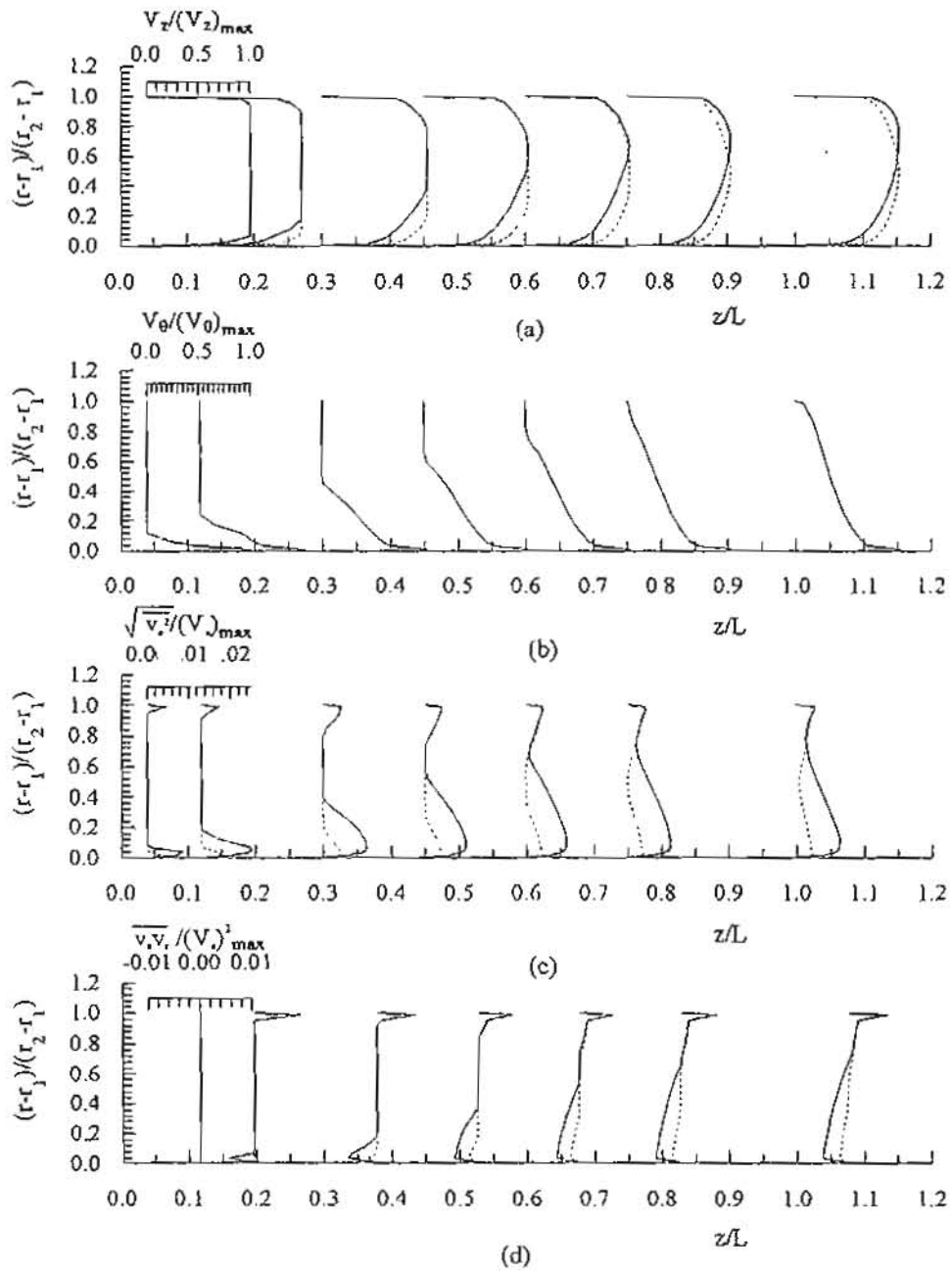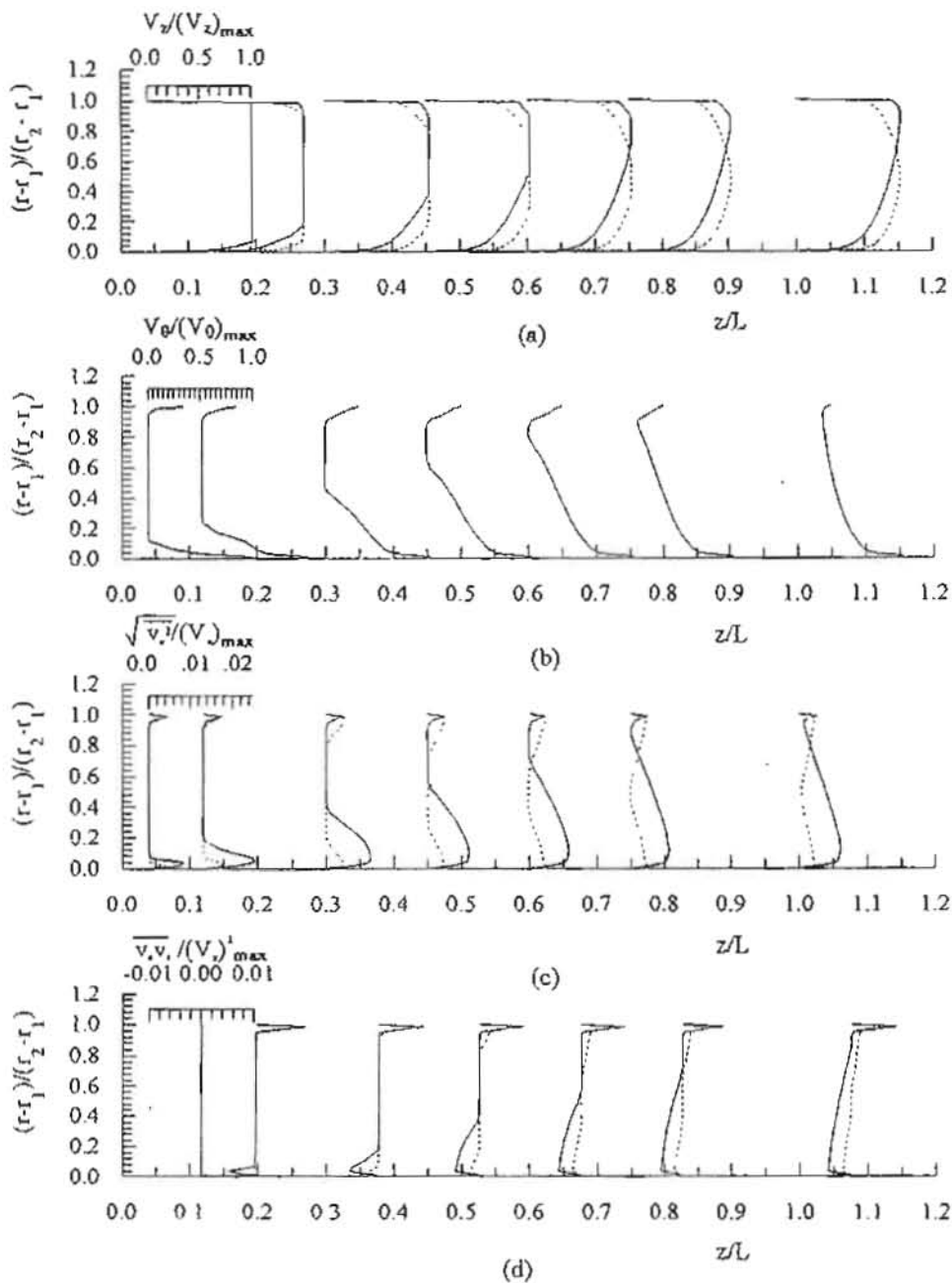for outer cylinder rotating only $\omega_1 = 0$.
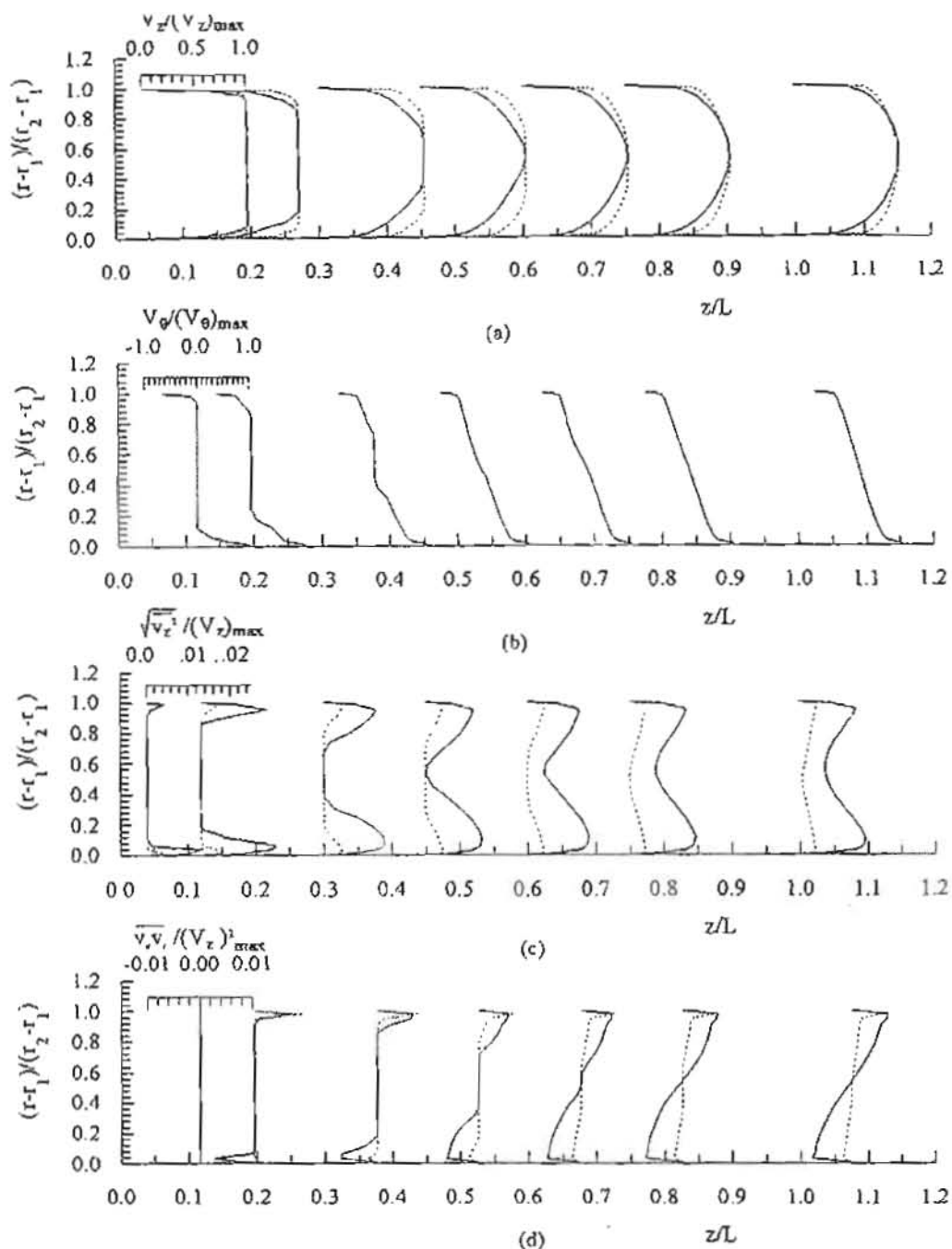
Figure (3) Development of the flow with the downstream distance for radius
ratio = 0.75 with aspect radio = 50.0 and R_c= 6.22 X 10^5 at α = –2.0

———— Rotating Cylinders.   ·············· Stationary cylinders.
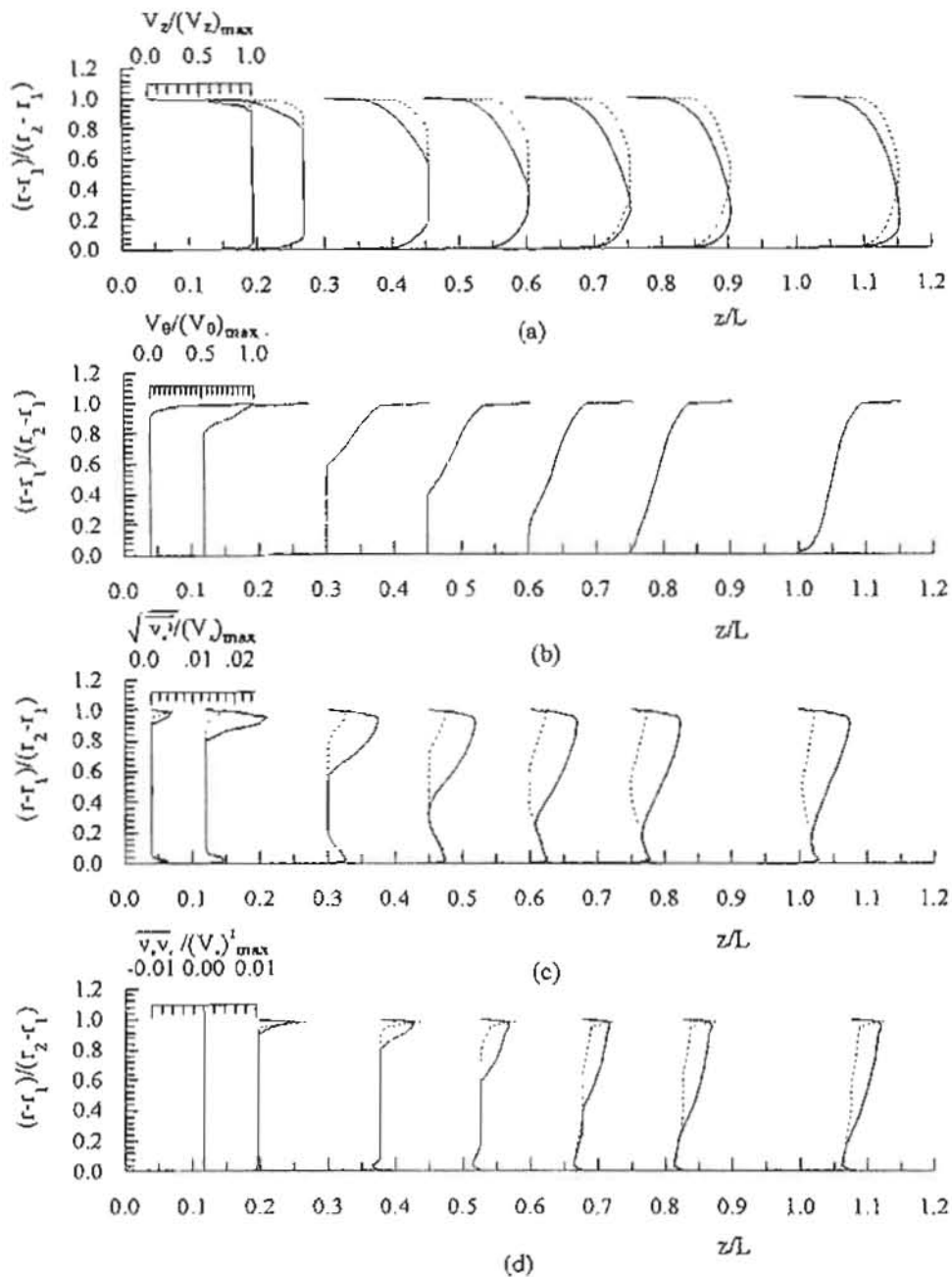
Figure (4) Development of the flow with the downstream distance for radius
ratio = 0.75 with aspect radio = 50.0 and R_e = 6.62 X 10^5 at ω_1 = 0.0
———— Rotating cylinders.   ·············· Stationary cylinders.

Figure (5) Development of the flow with the downstream distance for radius ratio = 0.75 with aspect radio = 50.0 and R_e= 6.62 X 10^5 at ω_2= 0.0 & ω_1= 10.
——————— Rotating cylinders.   .... Stationary cylinders.

Figure (6) Development of the flow with the downstream distance for radius ratio = 0.75 with aspect radio = 50.0 and R_e= 6.62 X 10^5 at α = 4.0

——————— Rotating cylinders.   ················· Stationary cylinders.
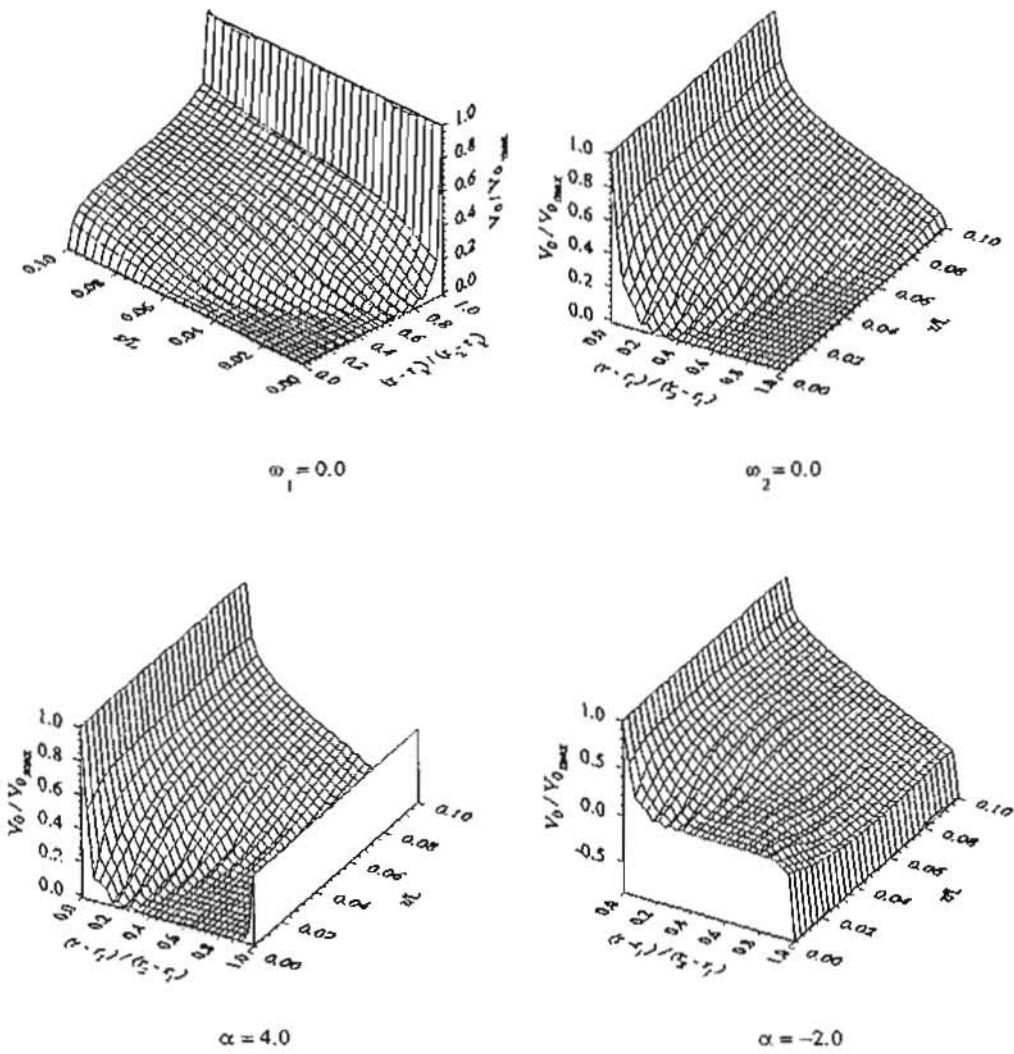
Figure (7) Three-dimensional representation of the predicted tangintial mean velocity
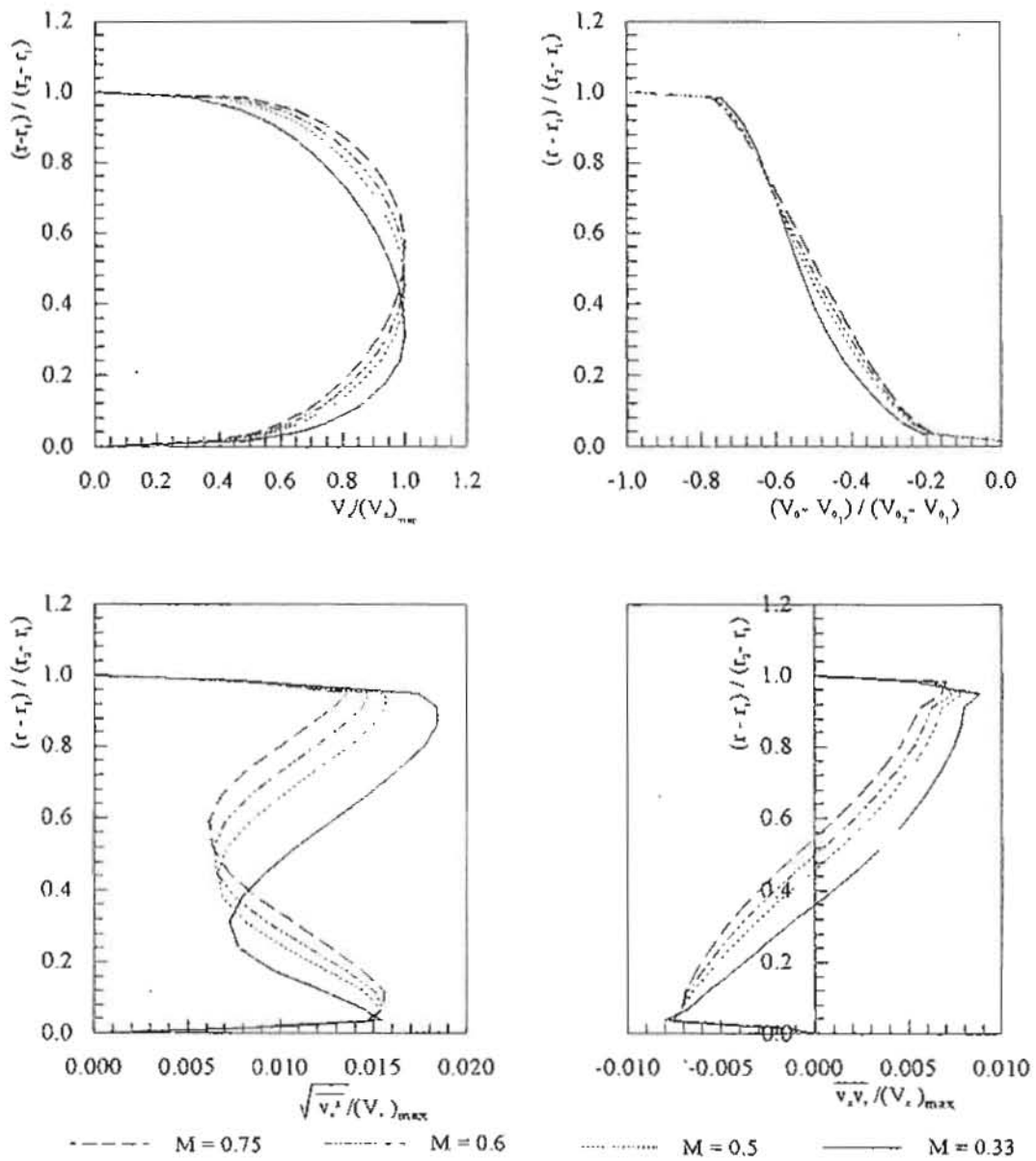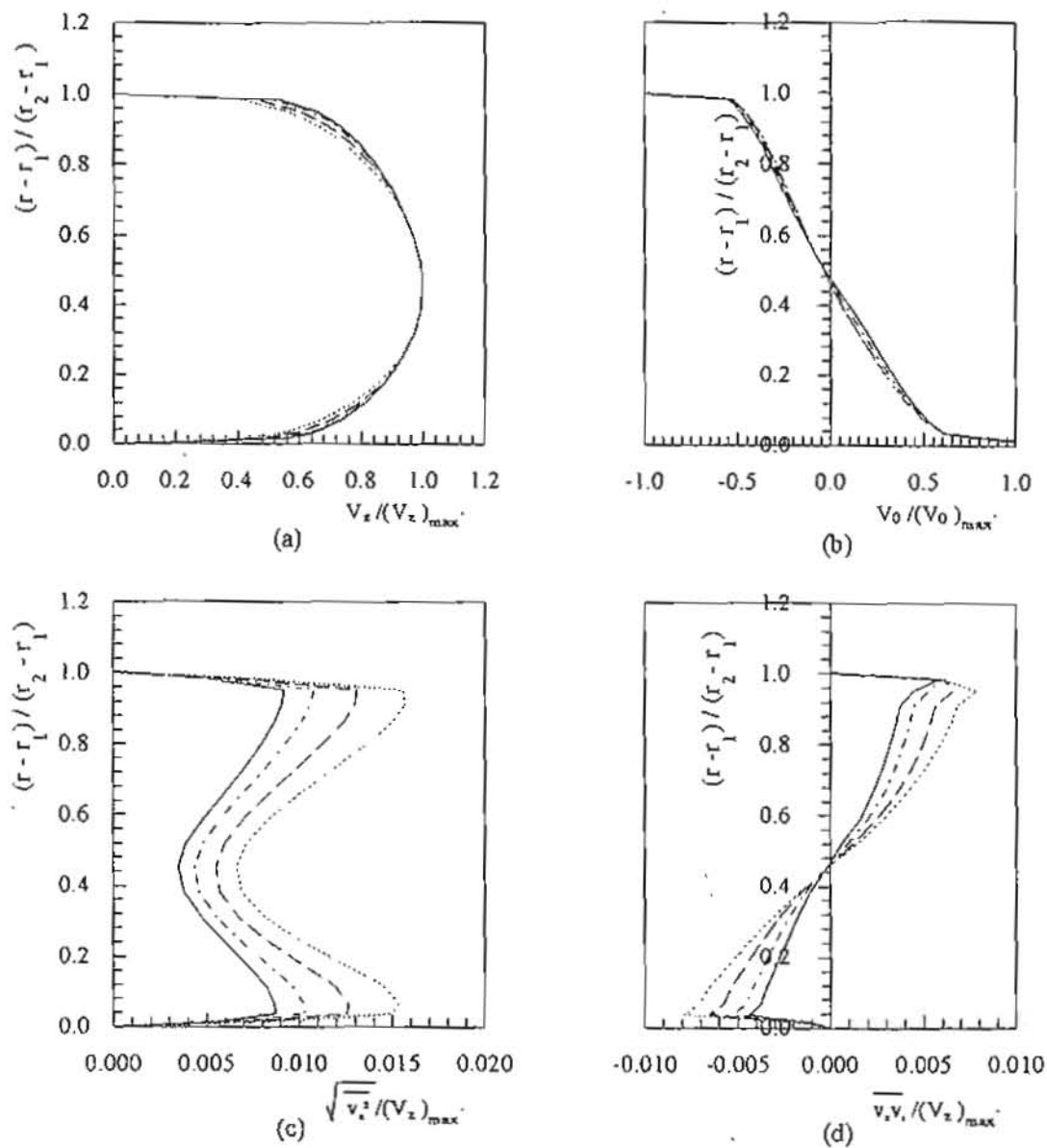for different angular velocity ratios at radius ratio = 0.6 and $R_e = 6.62 \times 10^5$

·---- M = 0.75   ·------ · M = 0.6   ·········· M = 0.5   ——— M = 0.33

Figure (8) Variation of fully developed flow parameters with radius ratio
at aspect ratio = 50 & $\omega_1 / \omega_2 = -2.0$.

Figure (9) Variation of flow parameters with Reynolds number for fully developed
flow at aspect ratio = 33 & R_1/R_2= 0.5 and ω_1/ω_2= 0.5 :

a) Axial mean velocity.   b) Tanginial mean velocity
c) Turbulence intensity distribution.   d) Shear stress distribution